AIAA JOURNAL
Vol. 39, No. 6, June 2001

Numerical Study of Cylindrical Blast-Wave Propagation and Reflection

Shen-Min Liang,* Ju-Lung Hsu,† and Jung-Sheng Wang†
National Cheng-Kung University, Tainan 701, Taiwan, Republic of China

The problem of an unsteady cylindrical blast-wave interaction with a flat plate is numerically investigated. The numerical simulation aims at the understanding of blast-wave propagation, reflection, and its transition phenomenon as well as the flow features induced by the blast wave. A fifth-order weighted essentially nonoscillatory scheme for spatial discretization associated with a fourth-order Runge–Kutta method for time integration is employed for solving the two-dimensional Euler/Navier–Stokes equations in a finite volume fashion. To verify the accuracy of the numerical solver developed, several problems were tested. The computed results for the test problems are shown to be accurate in comparison with experimental data. To study the flowfield of a blast wave, the problem of blast-wave propagation in a free field is explored first. Two types of initial conditions are considered. A contact-surface instability that developed around a contact surface was found in the problem with the first kind of initial condition. Next, the problem of the blast-wave interaction with the flat plate is investigated. The flow structure of a shock-shock interaction induced by the unsteady blast wave and its evolution are studied in detail. It was found that the lower the height of burst or the higher the shock Mach number, the earlier the occurrence of the transition from a regular reflection to a Mach reflection and the higher the triple points.

Introduction

THE interaction problem of an unsteady cylindrical blast wave with a flat plate is considered because the understanding of the unsteady blast-wave interaction is helpful both to structural engineers and to aerodynamicists. The structural engineers have interest in the transient blast loading effects. The aerodynamicists have interest in the flow structure induced by the blast wave and in the type of blast-wave reflection.

The flowfield induced by a spherical blast wave may contain one or more shock waves, expansion waves, and a contact surface. The primary shock wave is the first outward-moving wave and is followed by expansion waves. Thus the first shock wave causes an overpressure, and the expansion waves an underpressure. The following expansion waves can induce a secondary shock wave. An unsteady blast wave interaction with a flat plate is more complicated than an unsteady shock wave interaction with a flat plate because the strength of the first shock wave is changing during propagation. A cylindrical blast wave is primarily similar to that for the spherical case. Thus the present study will also be helpful for understanding the spherical blast waves' propagation.

In the recent 20 years there were very few papers that reported the detailed flow structure induced by a blast wave. Dewey et al.[1] experimentally studied the blast-wave interaction with a smooth surface and with a rough surface. They found that a smooth surface induces a stronger Mach stem and a higher triple-point trajectory. Takayama and Sekiguchi[2] studied the interaction of a blast wave with a cone surface and with a flat plate. They reported that the difference between analytic and experimental results for the flat plate case becomes large as the half wedge angle is increased. Colella et al.[3] numerically studied a high-explosive-driven blast-wave reflection using the Euler equations that were solved using a second-order Godunov scheme. They suggested that viscous effects should be included and that an adaptive grid be used. Hu and Glass[4] theoretically analyzed the type of blast-wave reflection at different heights of burst (HOB). When the HOB value is greater than some limit, there are only two types of shock-wave reflection: regular reflection (RR) and single Mach reflection (SMR). When the HOB value is less than this limit, there are four types of shock-wave reflection: RR, SMR, transitional-Machreflection (TMR), and double Mach reflection (DMR). Galkowski[5] used a one-dimensional model to study the RR $\Rightarrow$ MR transition for a strong spherical shock wave on a smooth plane. Dixon-Hiester et al.[6] experimentally investigated the RR $\Rightarrow$ MR transition region and its flow characteristic. Moreover, they observed that there is an abrupt pressure rise in the transition region. Ben-Dor[7] has classified the type of shock-wave reflection from a wedge in detail. Very recently, Jiang et al.[8] numerically and experimentally investigated micro-blast-wave propagation. They used a dispersion-controlled scheme for numerical simulation, and a similarity solution was used as an initial condition. There are many other papers that are related to shock/blast-wave propagation and reflection. Because of the space limitation, those papers are omitted here. Because numerical studies using a high-order solver for blast-wave propagation and reflection were limited, this study was made.

In this study both inviscid- and viscous-flow models are used for studying the blast-wave interaction problem. A fifth-order WENO (weighted essentially nonoscillatory) scheme with our extension to curvilinear coordinates and a fourth-order Runge–Kutta method of Jiang and Shu[9] are employed for discretizing the conservation equations of mass, momentum, and energy. The use of the fifth-order WENO scheme tends to avoid the need of using a very fine grid or adaptive grid for resolving flow discontinuities and large gradients. The working fluid is assumed to be air with $\gamma = 1.4$. We also assume that the flat plate is a smooth, adiabatic surface. To verify the accuracy of the solver developed, two problems of shock-wave reflection from a wedge were tested. After the code validation an unsteady blast wave in a free field is investigated for understanding the flow structure induced by the blast wave. Two kinds of initial conditions are considered. Finally a blast wave interacting with a smooth flat plate is explored for the transition phenomenon of the blast-wave reflection.

Mathematical Formulation and Numerical Method

Governing Equations

Neglecting the effects of external forces, the equations governing the blast-wave interaction with a flat plate are the continuity, momentum, and energy equations. It is assumed that the flow is laminar. In Cartesian coordinates (x, y) the dimensionless equations can be expressed in a conservative form as

$$\boldsymbol{Q}_1 + [\boldsymbol{F} - (1/Re)\boldsymbol{F}_v]_x + [\boldsymbol{G} - (1/Re)\boldsymbol{G}_v]_y = 0 \qquad (1)$$

Received 3 January 2000; revision received 28 December 2000; accepted for publication 5 January 2001.

*Professor, Institute of Aeronautics and Astronautics. Associate Fellow AIAA.
†Graduate Student, Institute of Aeronautics and Astronautics.

where subscripts t, x, y denote partial derivatives and subscript v denotes the viscous terms. $\boldsymbol{Q}$ is the conservative variable vector; $\boldsymbol{F}, \boldsymbol{G}$ the inviscid-flux vectors; $\boldsymbol{F}_v, \boldsymbol{G}_v$ the viscous flux vectors; and Re the Reynolds number. The Reynolds number is defined as the height of burst times the initial flow velocity behind the primary shock wave divided by the kinematic viscosity. The equation of state is needed to complete the system of equations (1). For more detail refer to Ref. 9. For easy treatment of boundary conditions, Eq. (1) is rewritten in curvilinear coordinates.

Numerical Method

Space Discretization and Time Integration

The numerical method of the high-order scheme of Jiang et al.[8] in a finite volume approach with an extension to curvilinear coordinates is used for solving Eq. (1). Basically the method consists of a fourth-order Runge–Kutta method for time integration and a fifth-order WENO scheme for spatial discretization. For more detail refer to Refs. 9–11. A local time step is chosen for unsteady flow calculations. The Courant–Friedrichs–Lewy value is set to be 0.5. All computations were performed on a Pentium II-400 with a 512-MB memory.

Initial and Boundary Conditions

The boundary conditions used are indicated in Fig. 1. The no-slip condition is imposed on the flat plate for the viscous-flow model and the tangency condition for the inviscid case. At the top and right boundaries the nonreflecting boundary condition of Thompson[12] is specified. A symmetric boundary condition is imposed at $x = 0$ to save computer memory and computation time.

Two kinds of initial conditions are considered. The first kind is a nonsimilarity solution[13] for a strong blast wave. The second kind is a flow whose construction is described next. The idea of the second kind of initial condition came from the blast wave generated by extracorporeal shock wave lithotriptors for treatment of kidney stones. For the second kind of initial flow condition, the pressure distribution remains the same as that in the similarity solution. The other flow properties such as the density and velocity behind the blast-wave front are determined by the Rankine–Hugoniot conditions with the given pressure distribution. Figure 2 shows the two kinds of initial condition as just described. The dashed lines denote the velocity, pressure, and density ratios in the first nonsimilar initial condition and the solid lines with symbols for the second kind. The pressure distribution for both cases is the same. Both the velocity and density distributions in the first kind of initial condition approach zero at the blast center. In the second kind of initial condition, the velocity and the density approach a finite, nonzero value of order one, respectively.

Results and Discussion

Code Validation

The Euler/Navier–Stokes solver developed here has been validated by comparing its predictions to results for various phenomena (e.g., shock-wave reflection from a wedge, a subsonic flow over a flat plate, the oblique shock interaction with a flat plate, and the propagation of an unsteady shock wave past a cylinder). Good agreement was evident. Clearly the present solver could resolve the four types of shock-wave reflection: RR, SMR, TMR, and DMR.[14] Only two types of shock-wave reflection are reported here, for which there were experimental data for comparison.

Figure 3 shows the computed densities on the wedge surface compared with the experimental data of Deschambault and Glass.[15] Figure 3a shows a single Mach reflection with $M_s = 2.05$ and

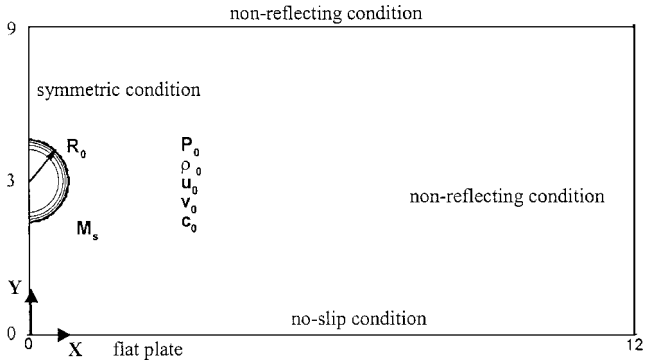

Fig. 1 Sketch of an initial blast-wave interaction with a flat plate.

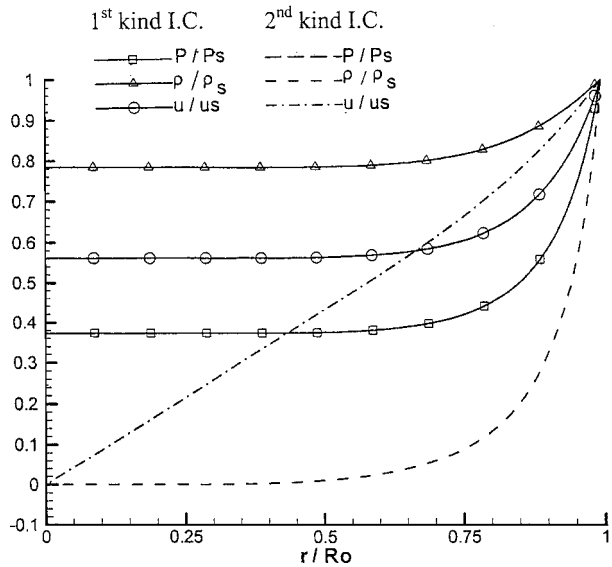

Fig. 2 Two kinds of initial condition chosen for numerical simulation of blast-wave propagation.

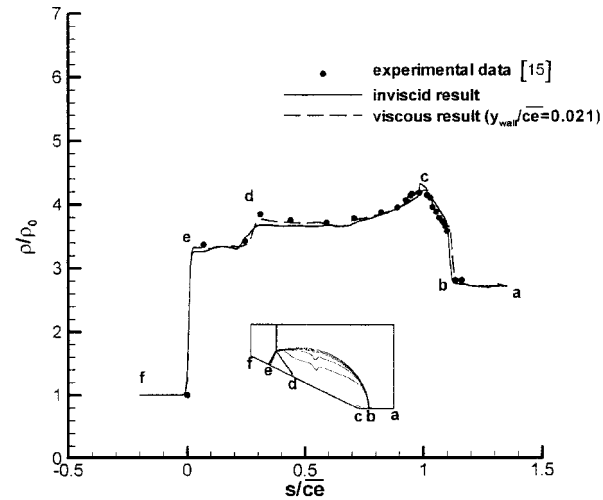

a) $M_s = 2.05$, $\theta_w = 63.4$ deg

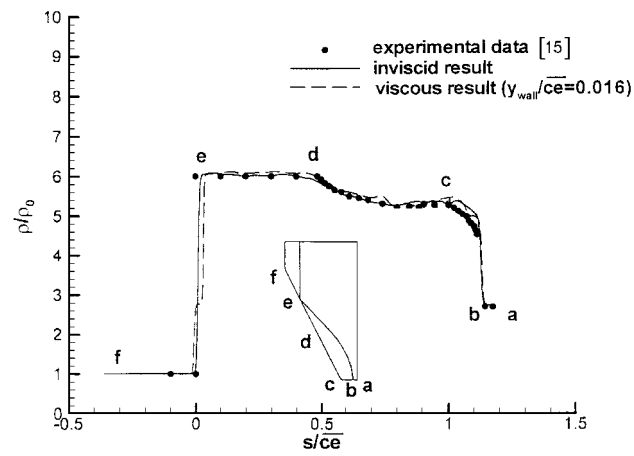

b) $M_s = 2.03$, $\theta_w = 27$ deg

Fig. 3 Comparison of computed density-ratio distributions with experimental data.

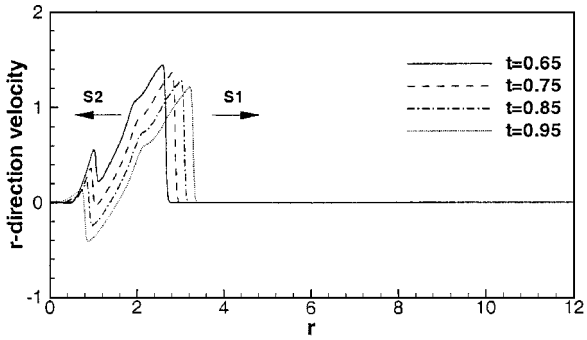

Fig. 4 Velocity distribution along the r direction ($y = 0$).

$\theta_w = 63.4$ deg, where M_s, θ_w denote the initially incident shock Mach number and the wedge angle, respectively. Figure 3b shows a regular reflection with $M_s = 2.03$ and $\theta_w = 27$ deg. We can see that the present results are in good agreement with the experimental data.

Blast-Wave Propagation in a Free Field

First we consider the case of the second kind of initial condition. The blast center is set to be $(x, y) = (0, 3)$. The computational domain is chosen to be $\{(x, y) \mid 0 < x < 12, -3 < y < 9\}$, and $M_s = 5$. The blast wave is assumed to have a radius of $R_0 = 0.5$. At the boundary of $x = 0$, a symmetry condition is imposed. At other boundaries $y = -3, 9$, and $x = 12$, a nonreflecting condition is imposed. A study of grid independence was made.[14] It was found that a 400×200 grid is accurate enough because a finer grid than this grid did not

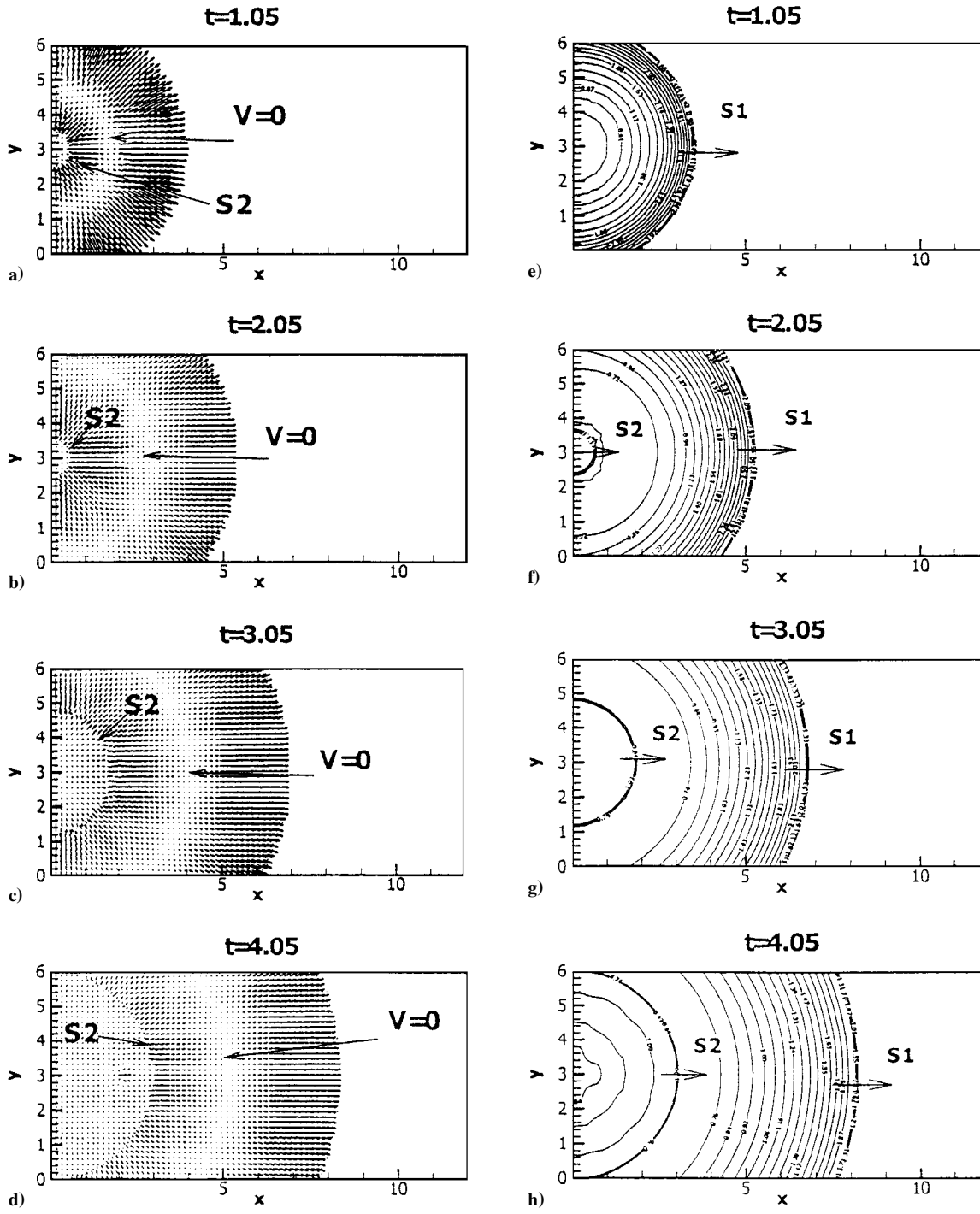

Fig. 5 Computed flowfields induced by a blast wave at different instants in a free field, $M_s = 5$: a–d) velocity fields and e–h) pressure-ratio contours.

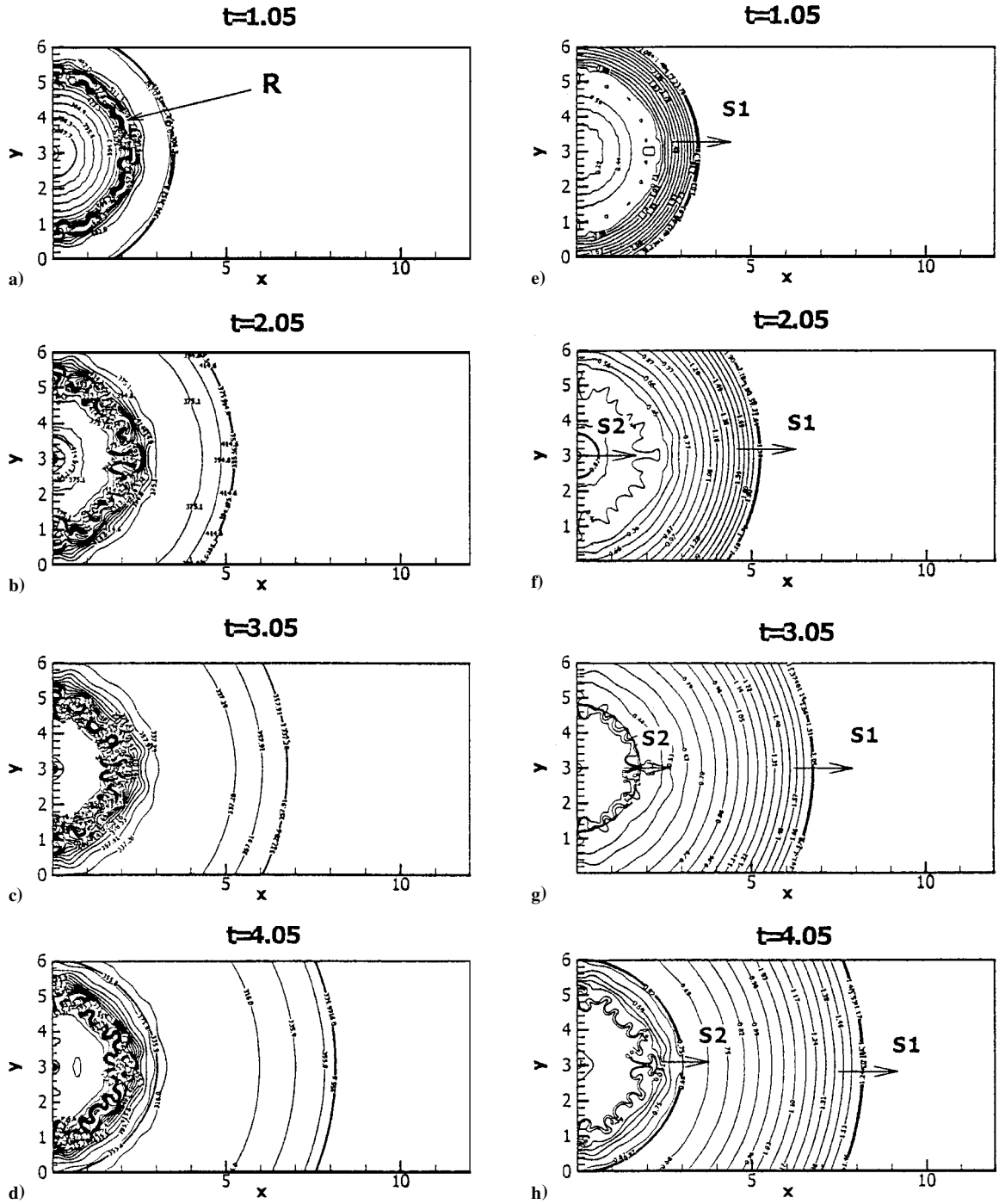

Fig. 6 Computed flowfields induced by a blast wave at different instants in a free field, $M_s = 5$: a–d) temperature contours and e–h) density-ratio contours.

significantly improve numerical solution. Flow properties reported next are dimensionless, except for the temperature. Figure 4 shows the velocity distributions along the r direction ($y = 3$). We can see that the flow velocities are all positive before $t \approx 0.75$. For $t > 0.75$ an inward-moving shock wave S_2 has been formed because of the development of some local negative velocities. The negative velocity means that the local flow moves inward and that a circular region of zero velocity has developed. This is because of the effect of the expansion waves that follow the primary outward-moving shock wave S_1. The change from a positive velocity to a negative velocity causes the development of a local circular region with near-zero velocity that contains the zero-velocity region. Figure 5 shows the velocity and pressure distributions at different instants. From Figs. 5a–5d one can clearly see the circular region of near-zero velocity and the inward-moving shock wave S_2 in Fig. 5a. The inward-moving shock S_2 will be reflected from the blast center at later times, as shown in Figs. 5b–5d. By examining the pressure distribution in Figs. 5f–5h, we can clearly see the primary and secondary outward-moving shocks.

Figure 6 shows the temperature and density distributions at different instants corresponding to Fig. 5. At $t = 1.05$ a circular region R of low density and high temperature has been developed, which is located approximately at $r = 2.2$. The maximum temperature ratio is about 2.32. At this moment the secondary shock is moving away from the region R. In particular, we find an interesting result of wave instability in the region R. The instability results from a contact surface where the density is discontinuous even though the pressure is continuous. The continuous pressure distribution can be seen from Fig. 5e. The contact-surface instability always exists for $t > 1.05$, as already shown in Figs. 5b–5d. The instability was not affected

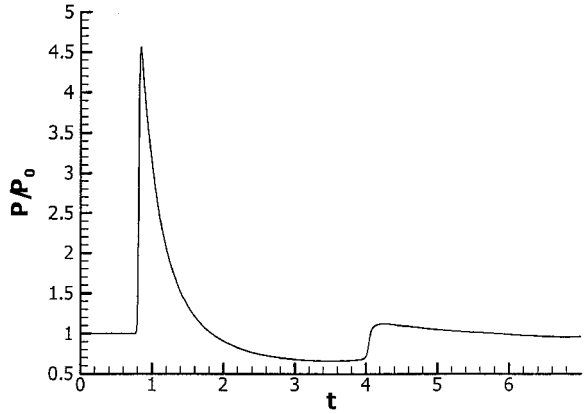

Fig. 7 Pressure ratio variations at the point (3.02, 3); $M_s = 5$.

by the flow viscosity or by the number of grid points. At $t = 2.05$ the secondary shock wave S_2 after reflection is moving outward, but has not yet arrived at the high-temperature region R. The maximum temperature ratio is 2.08. At $t = 3.05$ the secondary shock wave is passing through the high-temperature region, as shown in Fig. 5g. Consequently, the maximum temperature ratio is increased to 2.15. At $t = 4.05$ the secondary shock wave, having passed through the high-temperature region as shown in Figs. 5d and 5h, is located approximately at $r = 5$. The maximum temperature ratio is about 2.12. From Figs. 5a–5d we found an interesting phenomenon of wave instability. The instability did not grow with time, and the high-temperature region is oscillating at about $r = 2$. Because of the finite amplitude of the instability, the numerical solution did not diverge and could be obtained at any instant.

Figure 7 shows the pressure variation with respect to time at the point (3.02, 3). At $t = 0.8$ the first shock wave results in an abrupt pressure rise of about 4.55. Following the first shock front are the

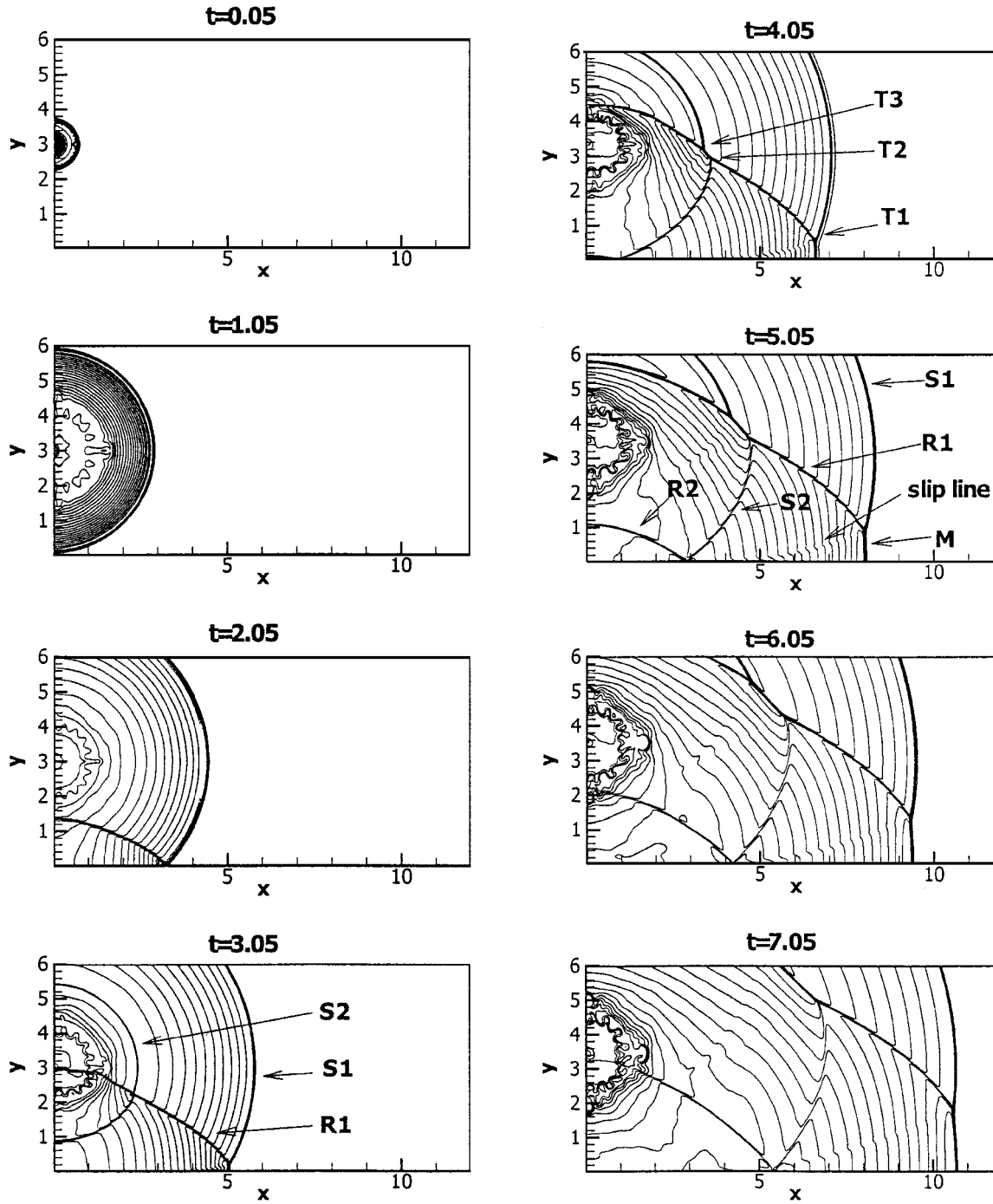

Fig. 8 Density and pressure fields induced by a blast-wave interaction with a flat plate at different instants; $M_s = 5$, HOB = 3.

expansion waves, causing a rapid pressure decrease. The pressure decrease consists two phases. The first one is a positive phase with a pressure greater than the undisturbed pressure p_0. The second is a negative phase with a pressure less than p_0. At approximately $t = 4.05$ the secondary shock wave S_2 propagates to this location, resulting in a pressure jump. Later on, the pressure decays to the undisturbed value p_0.

Next we consider the case of the first kind of initial condition, namely, a similarity solution as an initial condition. It was found that no secondary shock wave developed. This is because the initial density distribution is too low to develop an inward-moving shock wave within the region of $r \cong 0.75$, unlike the first case in which the initial density distribution is of order one so that local expansion can result in an inward-moving shock.

Blast-Wave Interaction with a Flat Plate

Consider an initial blast wave, located at $(x, y) = (0, 3)$, which is above the smooth, adiabatic flat plate at $y = 0$, as sketched in Fig. 1. The second kind of initial condition as described in the preceding section is used. The height of burst is chosen to be three. The study of grid independence was done using the Euler solver. Five grids—200×100, 300×150, 350×175, 400×200, 450×225—were used. They are referred as grid 1 to grid 5, respectively. It was found that the change with sequential grid refinement of the maximum surface pressure is 14, 4.7, 1.3, and 1.1%, respectively. Because the improvement from grid 4 to grid 5 is less than 1%, grid 4 was used for subsequent study. For viscous-flow calculations an additional 40 grid points in the y direction were added near the wall to grid 4. So a 400×240 grid was used for the viscous-flow calculations. The minimum y-direction spacing close to the wall is 0.003.

Both inviscid and viscous flows were calculated. The basic flow structure obtained from the viscous-flow model is almost the same as that from the inviscid-flow model. Thus only the inviscid-flow results are reported here.

Figure 8 shows the density ratio contours at different instants. At $t = 0.05$ the blast wave is expanding. At $t = 1.05$ the blast wave almost touches the flat plate. At $t = 2.05$ the type of shock-wave reflection is an RR type, and the reflected shock wave R_1 has not intersected the high-temperature region. At $t = 3.05$ the type of shock wave reflection becomes an SMR type. Meanwhile, the reflected shock wave R_1 intersects the secondary shock wave S_2 and penetrates into the high-temperature region. At $t = 4.05$ the intersection point of S_2 and R_1 has developed into two triple points denoted by T2 and T3, respectively. We believed that the mechanism of the development of two single-Mach reflections from a shock-shock interaction is caused by the interaction of two blast waves with nearly equal or equal shock strength, as reported in the paper of Dewey et al.[1] The verification of this point requires further study. At $t = 5.05$ the reflected shock wave S_2 has a RR-typed reflection with the secondary reflected shock R_2. At later times $t = 6.05$ and 7.05, the type of secondary shock-wave reflection remains the RR type. The reflected shock wave R_2 reaches the high-temperature region and penetrates it at later times.

The variation of the triple-point trajectory with HOB is shown in Fig. 9 for the case of $M_s = 5$. It can be seen that the lower the height of burst, the higher the triple point. These trajectories are not growing linearly. Some existing data at different shock Mach numbers have been included for reference. Moreover, the RR $\Rightarrow$ MR transition for smaller value of HOB occurs earlier than that for larger value of HOB.

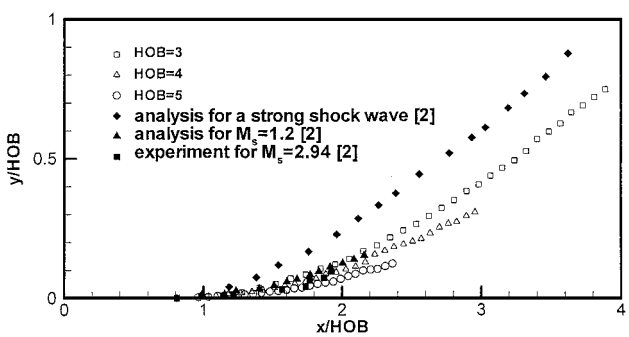

Fig. 9 Variations of the triple-point trajectory for different heights of burst; $M_s = 5$.

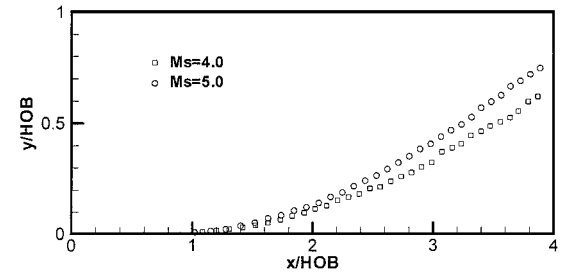

Fig. 10 Variations of the triple-point trajectory for different initial shock Mach numbers; HOB = 3.

By fixing the HOB value, the influence of the shock Mach number was investigated. Figure 10 shows the variation of the triple-point trajectory at $M_s = 4$ and 5. One can see that the higher the shock Mach number, the higher the triple point for a given HOB.

Conclusions

A reasonably accurate numerical solver has been developed and used to investigate the cylindrical blast-wave propagation and reflection. The present solver was validated using several test problems. After the code validation the blast-wave propagation in a free field is investigated in order to understand some particular flow structures induced by the blast wave. Two kinds of initial condition were studied. For the second kind of initial condition, namely, a nonsimilar solution, there is a secondary shock wave that moves inward at earlier times and then moves outward after reflection at later times. Moreover, a contact-surface instability occurred. The wave instability did not grow with time. Finally the blast-wave interaction with a smooth flat plate is investigated. The interaction of the reflection of the first shock wave with the secondary shock wave is studied. The shock-shock interaction can develop into two single-Mach reflections. The transition from the RR type to the SMR type for the first shock wave has been observed. It was found that the higher the shock Mach number or the lower the height of burst, the higher the triple point. However, the type of the secondary shock-wave reflection remains the RR type.

Acknowledgments

The support for this work under National Science Council Contract NSC 89-2612-E-006-018 is gratefully acknowledged. The authors also thank H. Chen for his computer drawing of some figures.

References

[1] Dewey, J. M., McMillin, D. J., and Classen, D. F., "Photogrammetry of Spherical Shocks Reflected from Real and Ideal Surfaces," *Journal of Fluid Mechanics*, Vol. 81, Pt. 4, Aug. 1977, pp. 701–717.

[2] Takayama, K., and Sekiguchi, H., "Formation and Diffraction of Spherical Shock Waves in a Shock Tube," Inst. of High Speed Mechanics, Tohoku Univ., Rept., Vol. 43, No. 336, 1981, pp. 89–119.

[3] Colella, P., Ferguson, R. E., Glaz, H. M., and Kuhl, A. L., "Mach Reflection from an HE-Driven Blast Wave," *Proceedings of the 10th International Colloquium on the Dynamics of Explosions and Reactive System*, AIAA, New York, 1986, pp. 388–421.

[4] Hu, T. C. J., and Glass, I. I., "Blast Wave Reflection Trajectories from a Height of Burst," *AIAA Journal*, Vol. 24, No. 4, 1986, pp. 607–610.

[5] Galkowski, A., "The Transition from Regular Reflection to Mach Reflection in the Problem of a Strong Spherical Shock Wave Acting on an Indeformable Perfectly Smooth Plane," *Journal of Technical Physics*, Vol. 28, No. 2, 1987, pp. 163–171.

[6] Dixon-Hiester, L. A., Reisler, R. E., Keefer, J. H., and Ethridge, N. H., "Shock Enhancement at Transition from Regular to Mach Reflection," *Proceedings of the 17th International Symposium on Shock Waves and Shock Tubes*, edited by W. K. Young, American Inst. of Physics, New York, 1990, pp. 204–209.

[7] Ben-Dor, G., *Shock Wave Reflection Phenomena*, Springer-Verlag, New York, 1992, p. 3.

[8]Jiang, Z., Takayama, K., Moosad, K. P. B., Onodera, O., and Sun, M., "Numerical and Experimental Study of a Micro-Blast Wave Generated by Pulsed-Laser Beam Focusing," *Shock Waves*, Vol. 8, No. 6, 1998, pp. 337–349.

[9]Jiang, G. S. and Shu, C.-W., "Efficient Implementation of Weighted ENO Schemes," *Journal of Computational Physics*, Vol. 126, No. 1, 1996, pp. 202–228.

[10]Shu, C. W., Zang, T. A., Erlebacher, G., Whitaker, D., and Osher, S., "High-Order ENO Schemes Applied to Two- and Three-Dimensional Compressible Flow," *Applied Numerical Mathematics*, Vol. 9, No. 1, 1992, pp. 45–71.

[11]Liu, X. D., Osher, S., and Chan, T., "Weighted Essentially Non-Oscillatory Schemes," *Journal of Computational Physics*, Vol. 115, No. 1, 1994, pp. 200–212.

[12]Thompson, W., "Time Dependent Boundary Conditions for Hyperbolic Systems," *Journal of Computational Physics*, Vol. 68, No. 1, 1987, pp. 1–24.

[13]Lin, S. C., "Cylindrical Shock Waves Produced by Instantaneous Energy Release," *Journal of Applied Physics*, Vol. 25, No. 1, 1954, pp. 54–57.

[14]Hsu, J. L., "Numerical Study of Blast-Wave Propagation on a Flat Plate," M.S. Thesis, Inst. of Aeronautics and Astronautics, National Cheng-Kung Univ., Tainan, Taiwan, ROC, June 1999.

[15]Deschambault, R. L., and Glass, I. I., "An Update on Non-Stationary Oblique Shock-Wave Reflections: Actual Isopycnics and Numerical Experiments," *Journal of Fluid Mechanics*, Vol. 131, June 1983, pp. 27–57.

M. Sichel
Associate Editor